catalysts

MDPI

Article

Surfactant- and Ligand-Free Synthesis of Platinum Nanoparticles in Aqueous Solution for Catalytic Applications

Rashmi P. Charde [1], Brian van Devener [2] and Michael M. Nigra [1,*]

[1] Department of Chemical Engineering, University of Utah, Salt Lake City, UT 84112, USA
[2] Electron Microscopy and Surface Analysis Laboratory, University of Utah, Salt Lake City, UT 84112, USA
* Correspondence: michael.nigra@utah.edu

Abstract: The synthesis of surfactant-free and organic ligand-free metallic nanoparticles in solution remains challenging due to the nanoparticles' tendency to aggregate. Surfactant- and ligand-free nanoparticles are particularly desirable in catalytic applications as surfactants, and ligands can block access to the nanoparticles' surfaces. In this contribution, platinum nanoparticles are synthesized in aqueous solution without surfactants or bound organic ligands. Pt is reduced by sodium borohydride, and the borohydride has a dual role of reducing agent and weakly interacting stabilizer. The 5.3 nm Pt nanoparticles are characterized using UV-visible spectroscopy and transmission electron microscopy. The Pt nanoparticles are then applied as catalysts in two different reactions: the redox reaction of hexacyanoferrate(III) and thiosulfate ions, and H_2O_2 decomposition. Catalytic activity is observed for both reactions, and the Pt nanoparticles show up to an order of magnitude greater activity over the most active catalysts reported in the literature for hexacyanoferrate(III)/thiosulfate redox reactions. It is hypothesized that this enhanced catalytic activity is due to the increased electron density that the surrounding borohydride ions give to the Pt nanoparticle surface, as well as the absence of surfactants or organic ligands blocking surface sites.

Keywords: platinum; sodium borohydride; H_2O_2 decomposition; hexacyanoferrate(III) ions; thiosulfate ions; catalysis

check for updates

Citation: Charde, R.P.; Devener, B.v.; Nigra, M.M. Surfactant- and Ligand-Free Synthesis of Platinum Nanoparticles in Aqueous Solution for Catalytic Applications. *Catalysts* **2023**, *13*, 246. https://doi.org/10.3390/catal13020246

Academic Editor: Stefania Specchia

Received: 21 December 2022
Revised: 13 January 2023
Accepted: 19 January 2023
Published: 21 January 2023

Copyright: © 2023 by the authors. Licensee MDPI, Basel, Switzerland. This article is an open access article distributed under the terms and conditions of the Creative Commons Attribution (CC BY) license (https://creativecommons.org/licenses/by/4.0/).

1. Introduction

Surfactants and covalently bound organic ligands often serve as stabilizing agents for metallic nanoparticles to protect against particle aggregation. While these molecules are effective at preventing particle aggregation, they can have detrimental effects in blocking surface sites which could be used for binding. Surfactants can often be displaced by other molecules which interact with the metallic surface more strongly, but organic ligands are often more difficult to displace. While it is possible to perform some reactions, such as benzyl alcohol oxidation [1–5] and CO oxidation [6], with organic ligands attached, many reactions, such as propylene epoxidation [7,8], oxidation of cyclohexane to cyclohexanol and cyclohexanone [9], and steam reforming of methane [10], require removal of at least some of the organic ligands from the metallic nanoparticle surface to observe catalytic activity. A comprehensive review by Fang et al. details the benefits and the drawbacks of ligands in heterogeneous catalytic systems [11].

In this contribution, platinum nanoparticles are synthesized in aqueous solution without the presence of surfactants, polymers, or covalently bound organic ligands on the Pt surface. A similar synthesis is reported by Astruc et al. for Au nanoparticles [12]. The Au nanoparticles, with an average size of 3.2 ± 0.8 nm, are used to catalyze 4-nitrophenol reduction in that work. We expect to synthesize Pt nanoparticles of a similar size in this work, as Au and Pt are chemically similar. Building upon their results, our synthesis method only requires a platinum salt such as chloroplatinic acid (H_2PtCl_6) and sodium borohydride for the synthesis of stable Pt nanoparticles in water. To our knowledge, these results

represent the first synthesis of Pt nanoparticles in aqueous solution without surfactants, polymers, or bound organic ligands in the literature. In organic solvent, Pt nanoparticles have been synthesized by Arenz et al. using ethylene glycol and NaOH as a reducing agent [13–15]. The authors modulate the ratio between NaOH and the Pt precursor salt to control the size of the resulting Pt nanoparticles to between 1 and 5 nm with precision, and they demonstrate the catalytic activity of these nanoparticles using the electrochemical oxygen reduction reaction. Quinson et al. have made several contributions in the synthesis of surfactant-free Pt nanoparticles in alkaline methanol [16–18] and ethanol [19]. There have also been a number of reviews published on surfactant- and ligand-free nanoparticle synthesis in the literature [20–22].

In our contribution, the Pt nanoparticles serve as catalysts for two different reactions. The first reaction is the electron-transfer reaction between hexacyanoferrate(III) ions and thiosulfate ions, and the second reaction is the decomposition of hydrogen peroxide. Hexacyanoferrate(III) ions form during gold mining processes when cyanide is used to extract Au, but co-located iron and other metals also form complexes with the cyanide [23]. H_2O_2 decomposition has great significance, as H_2O_2 can be used as an oxidant for many reactions, such as glucose oxidation [24–26], partial oxidation of methane [27–30], epoxidation of alkenes [7,8,31–34], wastewater treatment [35], and as a precursor for oxidative radicals in the presence of a Fenton catalyst [36–39], to name a few examples. Additionally, Pt catalysts have also been used as a H_2O_2 decomposition catalyst in contact lens cleaning solutions [40]. While there are many reports of catalyzed H_2O_2 synthesis in the literature, there are far fewer reports that investigate catalyzed H_2O_2 decomposition. We show that our Pt nanoparticles are active for both reactions, and that our Pt nanoparticles are approximately an order of magnitude more active than polymer-stabilized Pt nanoparticles for the redox reaction of hexacyanoferrate(III) and thiosulfate ions. Our Pt nanoparticles have similar activity to the most active Pt nanoparticles in the literature without the need of a stabilizing agent. In addition to the two specific reactions studied in this work, it is envisioned that these very active Pt nanoparticles could be used as catalysts for a wide variety of applications in aqueous solutions.

2. Results

2.1. Synthesis and Characterization

Platinum nanoparticles are synthesized through the reaction of H_2PtCl_6 with 10 equivalents of $NaBH_4$ in DI water at 25 °C. The Pt(IV) ions are reduced by the borohydride to Pt(0). This change can be observed in the UV-vis spectra that are shown in Figure 1. After reduction, the peak that is present in the H_2PtCl_6 corresponding to Pt(IV) at 260 nm is not observed in the Pt nanoparticles two hours after addition of $NaBH_4$. Additionally, the peak at 215 nm corresponding to unreduced Pt(II) cations [41] has decreased in size by 69% after two hours.

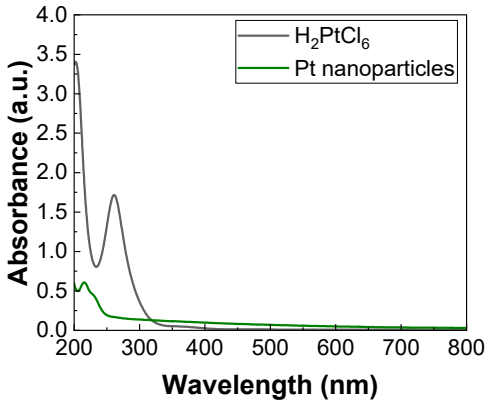


Figure 1. UV-vis spectra for H_2PtCl_6 (black) and the reduced Pt nanoparticles (green) in aqueous solution. The Pt nanoparticle solution spectra are taken two hours after $NaBH_4$ addition.

The particle size distribution of the synthesized Pt nanoparticles is measured using transmission electron microscopy (TEM). Figure 2A,C, and E show representative TEM images of the Pt nanoparticles at 2 h, 48 h, and 96 h reduction times, and Figure 2B,D, and F are the particle size distributions with those reduction times. The particle size distributions are obtained by measuring the size of over 100 nanoparticles in Figure 2B,D, and F. The average size of the nanoparticles synthesized are listed in Figure 2B,D,F. Additional TEM images showing the lattice fringes of the Pt nanoparticles and the electron diffraction pattern are shown in Figures S2 and S3, respectively. We observe in the sample that is reduced for 96 h the appearance of a significant number of much smaller nanoparticles, which are on average 1.2 nm in diameter. These very small nanoparticles are not observed in the samples with shorter reduction times. A small amount of Pt precipitation is also observed at 96 h in the samples. Our hypothesis is that, over time, the sodium borohydride reducing agent etches the Pt nanoparticles to decrease the observed average particle size and to form the smaller 1.2 nm Pt nanoparticles. Some of the 1 nm nanoparticles may be short-lived and aggregate to form very large particles. We did not observe nanoparticles which are > 20 nm in our microscopy studies of these samples. This etching behavior has been observed previously with Ag nanoparticles in the presence of $NaBH_4$ and dissolved oxygen, which are both present in our system [42].

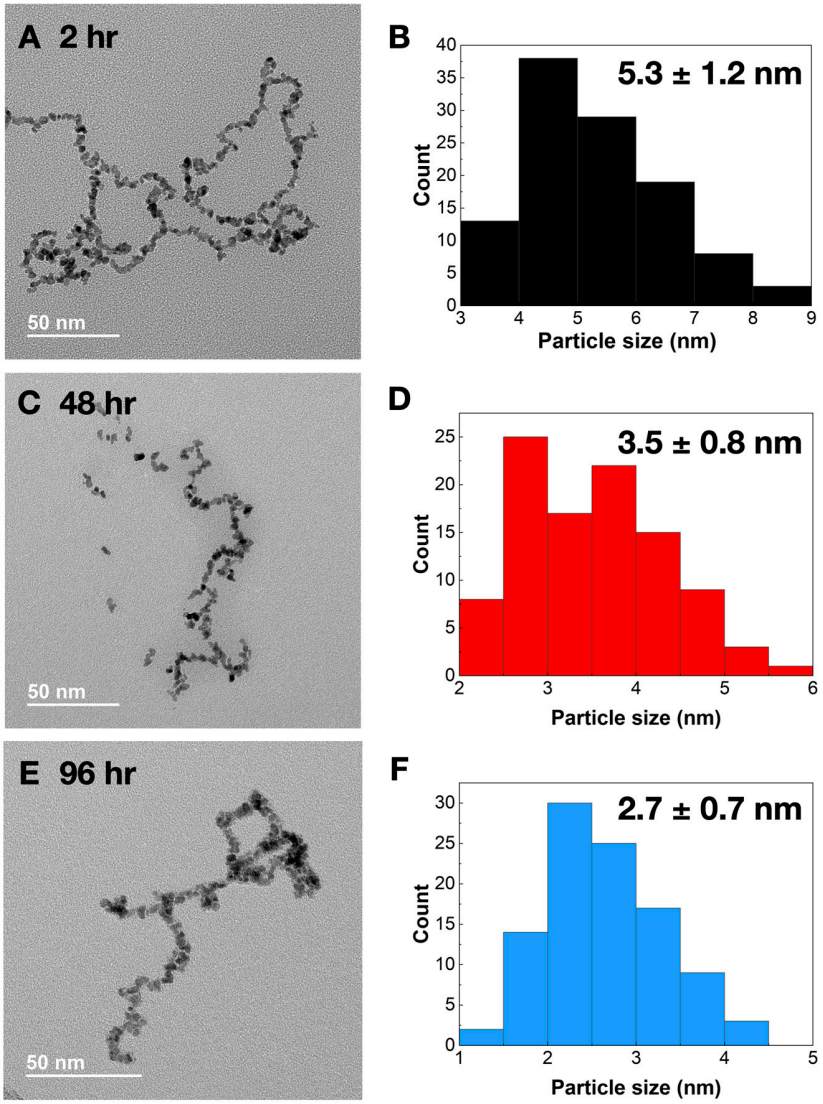


Figure 2. *Cont.*

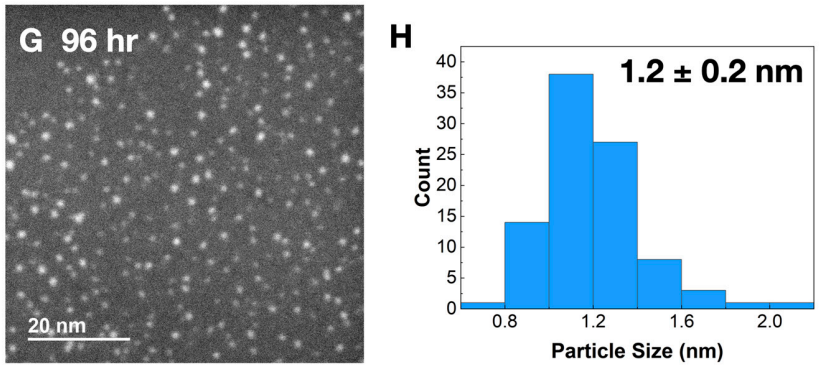


Figure 2. (**A**,**C**,**E**) Bright-field TEM image of synthesized Pt nanoparticles after 2, 48, and 96 h of reduction, respectively. (**B**,**D**,**F**) Particle size distribution histogram of synthesized Pt nanoparticles after 2, 48, and 96 h of reduction, respectively. The scale bar on panels A, C, and E represents 50 nm. The average particle sizes are listed on the particle size distributions. (**G**) High-angle annular dark-field scanning transmission electron microscopy (HAADF-STEM) image of small Pt nanoparticles after 96 h of reduction. These small particles are not included in the particle size distribution in panel F. The 1.2 nm particles are not observed in the samples reduced for 2 and 48 h. (**H**) Particle size distribution of the smallest particles observed at 96 h of reduction time.

To further assess the stability of the Pt nanoparticles over time, the UV-vis spectra over 96 h after borohydride addition are taken. In Figure 3, there are no significant shifts in the spectra; however, after 96 h, Pt nanoparticles start to visibly precipitate at the bottom of the storage vials, which is indicative of a loss of Pt nanoparticle stability over time.

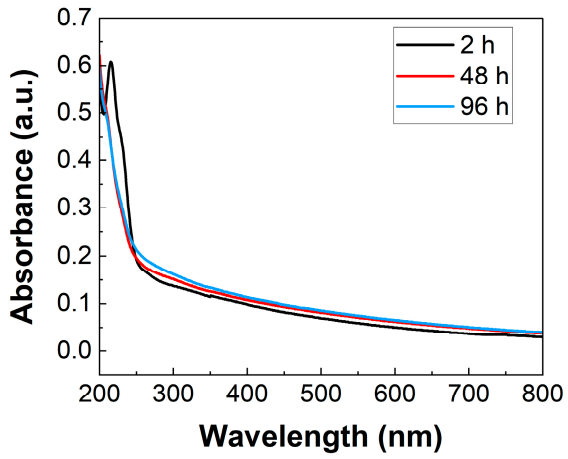


Figure 3. UV-vis spectra of Pt nanoparticles in aqueous solution at 2 h (black), 48 h (red), and 96 h (blue) after adding sodium borohydride.

2.2. Catalytic Reaction Testing

To test if the Pt nanoparticles exhibit catalytic activity, two reactions are chosen: the redox reaction between hexacyanoferrate(III) ions and thiosulfate ions, and H_2O_2 decomposition. These reactions are selected for their ease of monitoring using UV-vis in the case of the first reaction, and their high industrial/environmental importance in the case of H_2O_2 decomposition. The reaction between hexacyanoferrate(III) and thiosulfate occurs according to Equation (1) with a Pt catalyst.

$$2\ Fe(CN)_6^{3-} + 2\ S_2O_3^{2-} \rightarrow 2\ Fe(CN)_6^{4-} + S_4O_6^{2-} \quad (1)$$

Hydrogen peroxide decomposition occurs in the presence of a Pt catalyst according to Equation (2).

$$2\ H_2O_2 \rightarrow 2\ H_2O + O_2 \quad (2)$$

The results of the electron-transfer reaction between thiosulfate ions and hexacyanoferrate(III) ions are illustrated in Figure 4 over the course of 30 min of reaction time. The reaction is monitored by observing the absorbance at 420 nm corresponding to the concentration of hexacyanoferrate(III) ions [43]. The calibration is shown in Figure S1. In this regime of high thiosulfate concentration relative to hexacyanoferrate(III) concentration, the reaction can be assumed to be pseudo-first-order in $[Fe(CN)_6^{3-}]$ [43]. In the literature, Narayanan and El-Sayed use PVP-stabilized Pt nanoparticles as a catalyst for this same electron-transfer reaction. They observe a rate constant of 0.142 min^{-1} (mg of Pt)$^{-1}$ using 4.8 nm tetrahedral nanoparticles, which is reported over an average of temperatures between 25 °C and 45 °C [43]. We observe a rate constant of 1.58 min^{-1} (mg of Pt)$^{-1}$, which is calculated from the slope in Figure 4. Our average particle size (5.3 nm) is slightly larger than the 4.8 nm particle size reported by Narayanan and El-Sayed [43]. The fraction of surface atoms on the 4.8 nm and 5.3 nm particles is estimated to be within 10% of each other as shown in SI Section 4. Thus, for approximately the same number of surface sites, we report approximately an order of magnitude increase in reaction rate constant. Additionally, our rate is measured only at 25 °C, while Narayanan and El-Sayed report their rate averaged between temperatures of 25 °C and 45 °C. Based on the activation energy reported for this reaction by Narayanan and El-Sayed of 14 kJ/mol, the rate constant could increase by a factor of 1.4 times between 25 °C and 45 °C when using the Arrhenius equation to calculate rate constants at different temperatures. This would put our rate constant, on a per surface Pt atom basis, over an order of magnitude greater. Table S2 shows a comparison between the different Pt-catalyzed rate constants found in the literature, and our catalysts are at least an order of magnitude greater in activity. At least a factor of three increase in rate is also observed by Astruc et al. when using borohydride-stabilized Au nanoparticles for 4-nitrophenol reduction when compared to Au nanoparticles that are stabilized with other species. All except one of the catalysts which Astruc et al. use as a comparison are an order of magnitude less active than the borohydride-stabilized Au nanoparticles [12].

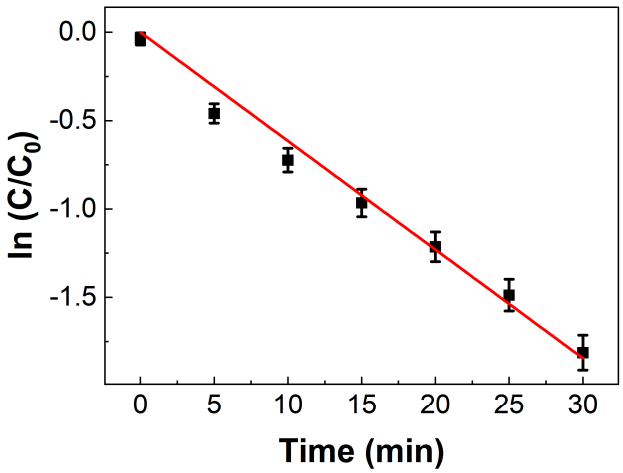


Figure 4. Pseudo-first-order reaction rate plot for electron-transfer reaction between hexacyanoferrate(III) and thiosulfate ions. The initial concentration of hexacyanoferrate(III) is 10^{-3} M, and the initial concentration of thiosulfate is 0.2 M. The Pt concentration is 65.8 μM. The reaction takes place at 25 °C.

Looking at the second reaction of our study, many transition metals such as Pt, Pd, Ir, Ru, and Au are active catalysts for H_2O_2 decomposition, and Pt is known to be the most active metal for this reaction [44]. H_2O_2 decomposition is catalyzed at two different pH values, 7 and 10, by our borohydride-stabilized Pt nanoparticles at 25 °C. The rate of reaction is determined by acidified $Ce(SO_4)_2$ titrations, as has been utilized previously

in the literature to measure H_2O_2 synthesis and decomposition rates [27,45–47]. Further details of the titrations are included in Section 3.5.

H_2O_2 decomposition is pseudo-first-order in H_2O_2 concentration under the reaction conditions in our work [40,48–50] as illustrated in Figure 5. Figure 5A and B show first order H_2O_2 decomposition kinetics at pH 7 and pH 10, respectively. It is known that H_2O_2 decomposition rates are higher in more alkaline solutions [24,44,49,51,52]. Our results show that this is also the case for these Pt nanoparticles. At pH 7, the rate constant is 1.53 min^{-1} $(mg\ Pt)^{-1}$, while at pH 10 the rate constant observed is 7.18 min^{-1} $(mg\ Pt)^{-1}$. These rates are calculated from the slopes in Figure 5A,B. Stach et al. [53], in an extensive study, evaluated H_2O_2 decomposition rates in three different Pt catalysts: Pt nanopowder, Pt black, and 3 nm polymer-stabilized colloidal Pt nanoparticles. Using the rate equation that Stach et al. developed for the 3 nm polymer-stabilized particles, when the rate is calculated using our reaction temperature and H_2O_2 concentration, their rate is shown to be 0.00239 $mol/(m^2min)^{-1}$ in ESI Section 4. If our rate is normalized to Pt surface area, we obtain a rate of 0.0568 $mol/(m^2min)^{-1}$ at pH 7 and a rate of 0.266 $mol/(m^2min)^{-1}$ at pH 10. At our lowest rate, measured at pH 7, we are more than an order of magnitude greater than the 3 nm particles. It may not have been expected that our larger 5.3 nm particles would be much more active on a per surface area basis than the 3 nm particles, but Stach et al. hypothesize that larger particles have a lower work function, which provides a higher electron density to the adsorbates [53]. Additionally, according to Weiss [54], the first step in H_2O_2 decomposition is the transfer of an electron from the metal surface to H_2O_2 to form OH and HO_2 radicals. An electron-rich surface would enable this critical step in the mechanism. Following this hypothesis, we would expect Pt black, which has 11.3 nm particles, to be more active than the 5.3 nm particles. However, Pt black has a rate of 0.0303 $mol/(m^2min)^{-1}$, which is lower than we observe for the 5.3 nm particles synthesized in this work. At larger nanoparticle sizes of 22.7 nm in Pt nanopowder, the effect of particle size is greater on the catalytic activity than the electronic effect, and a rate of 0.123 $mol/(m^2min)^{-1}$ is observed. Based on these results, we hypothesize that our 5.3 nm particles are more active than Pt black due to the electron-rich borohydride ions that surround the Pt nanoparticles, increasing the electronic density on the Pt surface [12]. A detailed comparison of the decomposition rates for various sizes of nanoparticles is included in Table S1. The most active Pt nanoparticles that we found in the literature are supported on to acrylonitrile-butadiene-styrene (ABS) polymer and coated with PDA (polydopamine) polymer, where, at pH 7, they achieved a rate constant of 2.48 min^{-1} $(mg\ Pt)^{-1}$ [55]. Our catalysts achieve close to that rate at pH 7, and even higher rates at pH 10. All other Pt-catalyzed rates reported in the literature, except those by Ohkubo et al. [55–57], are at least an order of magnitude less than our value at pH 7 of around 298K.

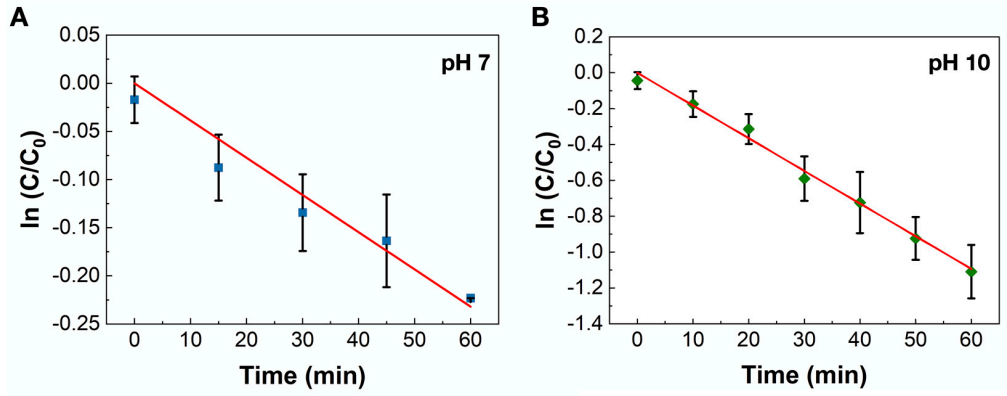


Figure 5. Pseudo-first-order reaction rate plots for H_2O_2 decomposition at (**A**) pH 7 (**B**) pH 10. The initial concentration of H_2O_2 is 100 mM. Pt concentration is 1.3 µM. Reaction rates are measured at 25 °C.

3. Materials and Methods

3.1. Chemicals and Reagents

Chloroplatinic acid (> 99.9%) and sodium borohydride were obtained from Sigma Aldrich (St. Louis, MO, USA). Hydrogen peroxide (30%) was obtained from Fisher Scientific (Fair Lawn, NJ, USA). Cerium (IV) sulfate (99%) and sodium thiosulfate pentahydrate (99%) were obtained from Thermo Scientific (Fair Lawn, NJ, USA). Sulfuric acid (95.7%) was obtained from Mallinckrodt (Paris, KY, USA). Potassium hexacyanoferrate(III) (98%) was obtained from Alfa Aesar (Heysham, UK) and ferroin indicator was obtained from Honeywell (Seelze, Germany).

3.2. Platinum Nanoparticle Synthesis

For this synthesis, methods from Astruc et al. were modified from their synthesis of stabilizer-free Au nanoparticles to use for the synthesis of Pt nanoparticles in this paper [12]. In our synthesis, 1.1 mg H_2PtCl_6 was dissolved in 20 mL of 18.2 MΩ water to make a 0.13 mM Pt solution. A total of 10 equivalents of $NaBH_4$ were added to the Pt precursor solution in one shot while the Pt solution was stirred. After adding the $NaBH_4$, the solution was stirred for 2 h. The UV-vis spectra in Figures 1 and 3 (at 2 h) were taken 2 h after $NaBH_4$ was added.

3.3. UV-Vis Spectroscopic Measurements

UV-vis spectroscopic measurements were taken using a Shimadzu UV-2600 spectrophotometer (Shimadzu, Kyoto, Japan) with 1 nm step size scanning from 800 nm to 200 nm. The spectra were recorded from the synthesis solution without further dilution.

3.4. Transmission Electron Microscopy Measurements

TEM measurements were recorded using bright-field mode with a JEOL JEM 2800 electron microscope (JEOL, Tokyo, Japan) at the Electron Microscopy and Surface Analysis Laboratory at the University of Utah. All measurements were obtained using an acceleration voltage of 200 keV and probe current of 1 nA. The PtNP solution was drop-casted on copper TEM grids and dried before obtaining the electron micrographs.

3.5. Pt-Catalyzed Hydrogen Peroxide Decomposition

The H_2O_2 decomposition reactions were performed at 25 °C. An amount of 20 mL of 100 mM H_2O_2 solution was added to a vial, and then 200 µL of 0.13 mM PtNP solution was added. The amount of H_2O_2 was calculated using the $Ce(SO_4)_2$ titration methods utilized by Hutchings et al. [45–47]. Specifically for the titrations, 50 mL of 0.9 N H_2SO_4 solution was taken in a conical flask, and ferroin indicator was added. This solution was titrated against 5 mM acidified $Ce(SO_4)_2$ until a pale blue color was seen. Aliquots of 100 µL of the reaction mixture were then added to the conical flask. The reaction sample containing H_2O_2 changed the color of the flask contents from pale blue to salmon. This was titrated until a pale blue color was seen. This was repeated every 10 min for the pH 10 reactions and every 15 min for the pH 7 reactions for 1 h. The reaction rate was calculated using the slopes in Figure S4.

3.6. Pt-Catalyzed Electron-Transfer Reaction between Hexacyanoferrate(III) and Thiosulfate Ions

For the electron-transfer reaction between hexacyanoferrate(III) ions and thiosulfate ions, 300 µL of 0.01 M potassium hexacyanoferrate(III) and 600 µL of 1 M sodium thiosulfate was added to 1.54 mL of 0.13 mM PtNP solution and 563 µL of 18.2MΩ DI water. The method used to detect the concentration of hexacyanoferrate(III) ions was published by Narayanan and El-Sayed [43]. The concentration of hexacyanoferrate(III) ions was measured using a Shimadzu UV-2600 spectrophotometer. The hexacyanoferrate(III) ions showed absorbance at 420 nm. There was a small amount of absorbance at 420 nm due to the Pt nanoparticles, and this was subtracted when the data were analyzed. The ab-

sorbance was monitored every 5 min for 30 min as shown in Figure S6. The reaction rate was calculated using the slope in Figure S5.

4. Conclusions

In summary, this contribution shows, for the first time, the synthesis of surfactant- and organic ligand-free Pt nanoparticles in aqueous solution. These Pt nanoparticles demonstrate over an order of magnitude enhanced activity for the redox reaction of hexacyanoferrate(III) ions and thiosulfate ions. They are also very active for H_2O_2 decomposition at pH 7 and pH 10, exhibiting over an order of magnitude higher activity than most of the Pt nanoparticle catalysts reported in the literature. It is hypothesized that the increased electron density the surrounding borohydride ions provide to the Pt increased the activity of the Pt nanoparticles. Based on these results, there is great potential to further apply these Pt nanoparticles for reactions that are accelerated by electron-rich Pt surfaces in aqueous solutions.

Supplementary Materials: The following supporting information can be downloaded at https://www.mdpi.com/article/10.3390/catal13020246/s1: Figure S1: Potassium hexacyanoferrate calibration curve; Figure S2: High magnification TEM images showing lattice fringes of Pt nanoparticles; Figure S3: Electron diffraction image for Pt nanoparticles after 2 h of reduction time; Figure S4: Pseudo-first-order reaction rate plots for H_2O_2 decomposition at pH 7 and pH 10; Figure S5: Pseudo-first-order reaction rate plot for electron-transfer reaction between hexacyanoferrate(III) and thiosulfate ions; Figure S6: Absorbance versus time plot for hexacyanoferrate(III) ions during reaction; Table S1: Pt catalyzed H_2O_2 decomposition rates in the literature; Table S2: Pt catalyzed hexacyanoferrate(III) and thiosulfate reaction rates in the literature [58–60].

Author Contributions: Conceptualization, R.P.C. and M.M.N.; methodology, R.P.C. and M.M.N.; validation, R.P.C. and M.M.N.; formal analysis, R.P.C. and M.M.N.; investigation, R.P.C., B.v.D., and M.M.N.; resources and writing, R.P.C. and M.M.N.; supervision, M.M.N.; project administration, M.M.N.; funding acquisition, M.M.N. and B.v.D. All authors have read and agreed to the published version of the manuscript.

Funding: R.P.C. and M.M.N. are grateful to the Department of Chemical Engineering at the University of Utah for funding this work. Additionally, this work made use of University of Utah shared facilities of the Micron Technology Foundation Inc. Microscopy Suite sponsored by the College of Engineering, Health Sciences Center, Office of the Vice President for Research, and the Utah Science Technology and Research (USTAR) initiative of the State of Utah. This work made use of University of Utah USTAR shared facilities supported, in part, by the MRSEC Program of the NSF under Award No. DMR-1121252.

Institutional Review Board Statement: Not applicable.

Informed Consent Statement: Not applicable.

Data Availability Statement: The data presented in this study are available in this article and in the supplementary information.

Conflicts of Interest: The authors declare no conflict of interest.

References

1. Zhou, Y.; Wang, Z.; Ye, B.; Huang, X.; Deng, H. Ligand effect over gold nanocatalysts towards enhanced gas-phase oxidation of alcohols. *J. Catal.* **2021**, *400*, 274–282. [CrossRef]
2. Yuan, S.-F.; Lei, Z.; Guan, Z.-J.; Wang, Q.-M. Atomically Precise Preorganization of Open Metal Sites on Gold Nanoclusters with High Catalytic Performance. *Angew. Chem. Int. Ed.* **2021**, *60*, 5225–5229. [CrossRef] [PubMed]
3. Brindle, J.; Sufyan, S.A.; Nigra, M.M. Support, composition, and ligand effects in partial oxidation of benzyl alcohol using gold–copper clusters. *Catal. Sci. Technol.* **2022**, *12*, 3846–3855. [CrossRef]
4. Tsunoyama, H.; Sakurai, H.; Negishi, Y.; Tsukuda, T. Size-Specific Catalytic Activity of Polymer-Stabilized Gold Nanoclusters for Aerobic Alcohol Oxidation in Water. *J. Am. Chem. Soc.* **2005**, *127*, 9374–9375. [CrossRef]
5. Sufyan, S.A.; van Devener, B.; Perez, P.; Nigra, M.M. Electronic Tuning of Gold Nanoparticle Active Sites for Reduction Catalysis. *ACS Appl. Mater. Interfaces* **2023**, *15*, 1210–1218. [CrossRef]

6. Wu, Z.; Hu, G.; Jiang, D.-e.; Mullins, D.R.; Zhang, Q.-F.; Allard, L.F.; Wang, L.-S.; Overbury, S.H. Diphosphine-Protected Au_{22} Nanoclusters on Oxide Supports Are Active for Gas-Phase Catalysis without Ligand Removal. *Nano Lett.* **2016**, *16*, 6560–6567. [CrossRef]
7. Kapil, N.; Weissenberger, T.; Cardinale, F.; Trogadas, P.; Nijhuis, T.A.; Nigra, M.M.; Coppens, M.-O. Precisely Engineered Supported Gold Clusters as a Stable Catalyst for Propylene Epoxidation. *Angew. Chem. Int. Ed.* **2021**, *60*, 18185–18193. [CrossRef]
8. Kapil, N.; Cardinale, F.; Weissenberger, T.; Trogadas, P.; Nijhuis, T.A.; Nigra, M.M.; Coppens, M.-O. Gold nanoparticles with tailored size through ligand modification for catalytic applications. *Chem. Commun.* **2021**, *57*, 10775–10778. [CrossRef]
9. Liu, Y.; Tsunoyama, H.; Akita, T.; Xie, S.; Tsukuda, T. Aerobic Oxidation of Cyclohexane Catalyzed by Size-Controlled Au Clusters on Hydroxyapatite: Size Effect in the Sub-2 nm Regime. *ACS Catal.* **2011**, *1*, 2–6. [CrossRef]
10. Cargnello, M.; Chen, C.; Diroll, B.T.; Doan-Nguyen, V.V.T.; Gorte, R.J.; Murray, C.B. Efficient Removal of Organic Ligands from Supported Nanocrystals by Fast Thermal Annealing Enables Catalytic Studies on Well-Defined Active Phases. *J. Am. Chem. Soc.* **2015**, *137*, 6906–6911. [CrossRef]
11. Lu, L.; Zou, S.; Fang, B. The Critical Impacts of Ligands on Heterogeneous Nanocatalysis: A Review. *ACS Catal.* **2021**, *11*, 6020–6058. [CrossRef]
12. Deraedt, C.; Salmon, L.; Gatard, S.; Ciganda, R.; Hernandez, R.; Ruiz, J.; Astruc, D. Sodium borohydride stabilizes very active gold nanoparticle catalysts. *Chem. Commun.* **2014**, *50*, 14194–14196. [CrossRef] [PubMed]
13. Quinson, J.; Inaba, M.; Neumann, S.; Swane, A.A.; Bucher, J.; Simonsen, S.B.; Theil Kuhn, L.; Kirkensgaard, J.J.K.; Jensen, K.M.Ø.; Oezaslan, M.; et al. Investigating Particle Size Effects in Catalysis by Applying a Size-Controlled and Surfactant-Free Synthesis of Colloidal Nanoparticles in Alkaline Ethylene Glycol: Case Study of the Oxygen Reduction Reaction on Pt. *ACS Catal.* **2018**, *8*, 6627–6635. [CrossRef]
14. Kacenauskaite, L.; Quinson, J.; Schultz, H.; Kirkensgaard, J.J.K.; Kunz, S.; Vosch, T.; Arenz, M. UV-Induced Synthesis and Stabilization of Surfactant-Free Colloidal Pt Nanoparticles with Controlled Particle Size in Ethylene Glycol. *ChemNanoMat* **2017**, *3*, 89–93. [CrossRef]
15. Quinson, J.; Dworzak, A.; Simonsen, S.B.; Theil Kuhn, L.; Jensen, K.M.Ø.; Zana, A.; Oezaslan, M.; Kirkensgaard, J.J.K.; Arenz, M. Surfactant-free synthesis of size controlled platinum nanoparticles: Insights from in situ studies. *Appl. Surf. Sci.* **2021**, *549*, 149263. [CrossRef]
16. Quinson, J.; Neumann, S.; Wannmacher, T.; Kacenauskaite, L.; Inaba, M.; Bucher, J.; Bizzotto, F.; Simonsen, S.B.; Theil Kuhn, L.; Bujak, D.; et al. Colloids for Catalysts: A Concept for the Preparation of Superior Catalysts of Industrial Relevance. *Angew. Chem. Int. Ed.* **2018**, *57*, 12338–12341. [CrossRef] [PubMed]
17. Quinson, J.; Kacenauskaite, L.; Bucher, J.; Simonsen, S.B.; Theil Kuhn, L.; Oezaslan, M.; Kunz, S.; Arenz, M. Controlled Synthesis of Surfactant-Free Water-Dispersible Colloidal Platinum Nanoparticles by the Co4Cat Process. *ChemSusChem* **2019**, *12*, 1229–1239. [CrossRef]
18. Quinson, J.; Mathiesen, J.K.; Schröder, J.; Dworzak, A.; Bizzotto, F.; Zana, A.; Simonsen, S.B.; Theil Kuhn, L.; Oezaslan, M.; Jensen, K.M.Ø.; et al. Teaching old precursors new tricks: Fast room temperature synthesis of surfactant-free colloidal platinum nanoparticles. *J. Colloid Interface Sci.* **2020**, *577*, 319–328. [CrossRef]
19. Quinson, J.; Neumann, S.; Kacenauskaite, L.; Bucher, J.; Kirkensgaard, J.J.K.; Simonsen, S.B.; Theil Kuhn, L.; Zana, A.; Vosch, T.; Oezaslan, M.; et al. Solvent-Dependent Growth and Stabilization Mechanisms of Surfactant-Free Colloidal Pt Nanoparticles. *Chem. A Eur. J.* **2020**, *26*, 9012–9023. [CrossRef]
20. Lu, L.; Zheng, H.; Li, Y.; Zhou, Y.; Fang, B. Ligand-free synthesis of noble metal nanocatalysts for electrocatalysis. *Chem. Eng. J.* **2023**, *451*, 138668. [CrossRef]
21. Reichenberger, S.; Marzun, G.; Muhler, M.; Barcikowski, S. Perspective of Surfactant-Free Colloidal Nanoparticles in Heterogeneous Catalysis. *ChemCatChem* **2019**, *11*, 4489–4518. [CrossRef]
22. Quinson, J. Colloidal surfactant-free syntheses of precious metal nanoparticles for electrocatalysis. *Curr. Opin. Electrochem.* **2022**, *34*, 100977. [CrossRef]
23. Arce-Sarria, A.; Aldana-Villegas, K.M.; Betancourt-Buitrago, L.A.; Colina-Márquez, J.Á.; Machuca-Martínez, F.; Mueses, M.A. Degradation of Hexacyanoferrate (III) from Gold Mining Wastewaters via UV-A/LED Photocatalysis Using Modified TiO_2 P25. *Water* **2020**, *12*, 2531. [CrossRef]
24. Brindle, J.S.; Nelson, P.S.; Charde, R.P.; Sufyan, S.A.; Nigra, M.M. Catalytic cooperativity between glucose oxidase and gold nanoparticles in the sequential oxidation of glucose to saccharic acid. *Green Chem.* **2022**, *24*, 5162–5170. [CrossRef]
25. Chen, J.; Ma, Q.; Li, M.; Chao, D.; Huang, L.; Wu, W.; Fang, Y.; Dong, S. Glucose-oxidase like catalytic mechanism of noble metal nanozymes. *Nat. Commun.* **2021**, *12*, 3375. [CrossRef] [PubMed]
26. Hermans, S.; Deffernez, A.; Devillers, M. Au–Pd/C catalysts for glyoxal and glucose selective oxidations. *Appl. Catal. A Gen.* **2011**, *395*, 19–27. [CrossRef]
27. Lewis, R.J.; Bara-Estaun, A.; Agarwal, N.; Freakley, S.J.; Morgan, D.J.; Hutchings, G.J. The Direct Synthesis of H_2O_2 and Selective Oxidation of Methane to Methanol Using HZSM-5 Supported AuPd Catalysts. *Catal. Lett.* **2019**, *149*, 3066–3075. [CrossRef]
28. Williams, C.; Carter, J.H.; Dummer, N.F.; Chow, Y.K.; Morgan, D.J.; Yacob, S.; Serna, P.; Willock, D.J.; Meyer, R.J.; Taylor, S.H.; et al. Selective Oxidation of Methane to Methanol Using Supported AuPd Catalysts Prepared by Stabilizer-Free Sol-Immobilization. *ACS Catal.* **2018**, *8*, 2567–2576. [CrossRef]

29. McVicker, R.; Agarwal, N.; Freakley, S.J.; He, Q.; Althahban, S.; Taylor, S.H.; Kiely, C.J.; Hutchings, G.J. Low temperature selective oxidation of methane using gold-palladium colloids. *Catal. Today* **2020**, *342*, 32–38. [CrossRef]
30. Agarwal, N.; Freakley, S.J.; McVicker, R.U.; Althahban, S.M.; Dimitratos, N.; He, Q.; Morgan, D.J.; Jenkins, R.L.; Willock, D.J.; Taylor, S.H.; et al. Aqueous Au-Pd colloids catalyze selective CH_4 oxidation to CH_3OH with O_2 under mild conditions. *Science* **2017**, *358*, 223–227. [CrossRef]
31. Huang, J.; Takei, T.; Ohashi, H.; Haruta, M. Propene epoxidation with oxygen over gold clusters: Role of basic salts and hydroxides of alkalis. *Appl. Catal. A Gen.* **2012**, *435-436*, 115–122. [CrossRef]
32. Huang, J.; Akita, T.; Faye, J.; Fujitani, T.; Takei, T.; Haruta, M. Propene epoxidation with dioxygen catalyzed by gold clusters. *Angew. Chem. Int. Ed. Engl.* **2009**, *48*, 7862–7866. [CrossRef] [PubMed]
33. Neurock, M.; Manzer, L.E. Theoretical insights on the mechanism of alkene epoxidation by H_2O_2 with titanium silicalite. *Chem. Commun.* **1996**, 1133–1134. [CrossRef]
34. Lu, X.; Zhou, W.-J.; Wu, H.; Liebens, A.; Wu, P. Selective synthesis of ethylene oxide through liquid-phase epoxidation of ethylene with titanosilicate/H_2O_2 catalytic systems. *Appl. Catal. A Gen.* **2016**, *515*, 51–59. [CrossRef]
35. Xu, J.; Zheng, X.; Feng, Z.; Lu, Z.; Zhang, Z.; Huang, W.; Li, Y.; Vuckovic, D.; Li, Y.; Dai, S.; et al. Organic wastewater treatment by a single-atom catalyst and electrolytically produced H_2O_2. *Nat. Sustain.* **2021**, *4*, 233–241. [CrossRef]
36. Agrawal, S.; Mysko, R.A.; Nigra, M.M.; Mohanty, S.K.; Hoepfner, M.P. Plasmonic Photocatalytic Enhancement of L-Cysteine Self-Assembled Gold Nanoparticle Clusters for Fenton Reaction Catalysis. *Langmuir* **2021**, *37*, 3281–3287. [CrossRef] [PubMed]
37. Liu, F.; Liu, Y.; Yao, Q.; Wang, Y.; Fang, X.; Shen, C.; Li, F.; Huang, M.; Wang, Z.; Sand, W.; et al. Supported Atomically-Precise Gold Nanoclusters for Enhanced Flow-through Electro-Fenton. *Environ. Sci. Technol.* **2020**, *54*, 5913–5921. [CrossRef]
38. Liu, S.; Wang, Y.; Wang, S.; You, M.; Hong, S.; Wu, T.-S.; Soo, Y.-L.; Zhao, Z.; Jiang, G.; Jieshan, Q.; et al. Photocatalytic Fixation of Nitrogen to Ammonia by Single Ru Atom Decorated TiO_2 Nanosheets. *ACS Sustain. Chem. Eng.* **2019**, *7*, 6813–6820. [CrossRef]
39. Thomas, N.; Dionysiou, D.D.; Pillai, S.C. Heterogeneous Fenton catalysts: A review of recent advances. *J. Hazard. Mater.* **2021**, *404*, 124082. [CrossRef]
40. Vetter, T.A.; Colombo, D.P. Kinetics of Platinum-Catalyzed Decomposition of Hydrogen Peroxide. *J. Chem. Educ.* **2003**, *80*, 788. [CrossRef]
41. van Wyk, P.-H.; Gerber, W.J.; Koch, K.R. A robust method for speciation, separation and photometric characterization of all $[PtCl_6-nBr_n]^{2-}$ (n=0–6) and $[PtCl_4-nBr_n]^{2-}$ (n=0–4) complex anions by means of ion-pairing RP-HPLC coupled to ICP-MS/OES, validated by high resolution 195Pt NMR spectroscopy. *Anal. Chim. Acta* **2011**, *704*, 154–161. [CrossRef] [PubMed]
42. Menumerov, E.; Hughes, R.A.; Golze, S.D.; Neal, R.D.; Demille, T.B.; Campanaro, J.C.; Kotesky, K.C.; Rouvimov, S.; Neretina, S. Identifying the True Catalyst in the Reduction of 4-Nitrophenol: A Case Study Showing the Effect of Leaching and Oxidative Etching Using Ag Catalysts. *ACS Catal.* **2018**, *8*, 8879–8888. [CrossRef]
43. Narayanan, R.; El-Sayed, M.A. Shape-Dependent Catalytic Activity of Platinum Nanoparticles in Colloidal Solution. *Nano Lett.* **2004**, *4*, 1343–1348. [CrossRef]
44. McKee, D.W. Catalytic decomposition of hydrogen peroxide by metals and alloys of the platinum group. *J. Catal.* **1969**, *14*, 355–364. [CrossRef]
45. Richards, T.; Lewis, R.J.; Morgan, D.J.; Hutchings, G.J. The Direct Synthesis of Hydrogen Peroxide Over Supported Pd-Based Catalysts: An Investigation into the Role of the Support and Secondary Metal Modifiers. *Catal. Lett.* **2022**, *153*, 32–40. [CrossRef]
46. Brehm, J.; Lewis, R.J.; Morgan, D.J.; Davies, T.E.; Hutchings, G.J. The Direct Synthesis of Hydrogen Peroxide over AuPd Nanoparticles: An Investigation into Metal Loading. *Catal. Lett.* **2022**, *152*, 254–262. [CrossRef]
47. Freakley, S.J.; Agarwal, N.; McVicker, R.U.; Althahban, S.; Lewis, R.J.; Morgan, D.J.; Dimitratos, N.; Kiely, C.J.; Hutchings, G.J. Gold–palladium colloids as catalysts for hydrogen peroxide synthesis, degradation and methane oxidation: Effect of the PVP stabiliser. *Catal. Sci. Technol.* **2020**, *10*, 5935–5944. [CrossRef]
48. Bianchi, G.; Mazza, F.; Mussini, T. Catalytic decomposition of acid hydrogen peroxide solutions on platinum, iridium, palladium and gold surfaces. *Electrochim. Acta* **1962**, *7*, 457–473. [CrossRef]
49. Serra-Maia, R.; Michel, F.M.; Douglas, T.A.; Kang, Y.; Stach, E.A. Mechanism and Kinetics of Methane Oxidation to Methanol Catalyzed by AuPd Nanocatalysts at Low Temperature. *ACS Catal.* **2021**, *11*, 2837–2845. [CrossRef]
50. MacInnes, D.A. The Mechanism of the Catalysis of the Decomposition of Hydrogen Peroxide by Colloidal Platinum. *J. Am. Chem. Soc.* **1914**, *36*, 878–881. [CrossRef]
51. Eley, D.D.; Macmahon, D.M. The decomposition of hydrogen peroxide catalysed by palladium-gold alloy wires. *J. Colloid Interface Sci.* **1972**, *38*, 502–510. [CrossRef]
52. Naya, S.-i.; Teranishi, M.; Kimura, K.; Tada, H. A strong support-effect on the catalytic activity of gold nanoparticles for hydrogen peroxide decomposition. *Chem. Commun.* **2011**, *47*, 3230–3232. [CrossRef] [PubMed]
53. Serra-Maia, R.; Winkler, C.; Murayama, M.; Tranhuu, K.; Michel, F.M. Abundance and Speciation of Surface Oxygen on Nanosized Platinum Catalysts and Effect on Catalytic Activity. *ACS Appl. Energy Mater.* **2018**, *1*, 3255–3266. [CrossRef]
54. Weiss, J. The catalytic decomposition of hydrogen peroxide on different metals. *Trans. Faraday Soc.* **1935**, *31*, 1547–1557. [CrossRef]
55. Ohkubo, Y.; Aoki, T.; Kaibara, D.; Seino, S.; Mori, O.; Sasaki, R.; Endo, K.; Yamamura, K. Strong Biomimetic Immobilization of Pt-Particle Catalyst on ABS Substrate Using Polydopamine and Its Application for Contact-Lens Cleaning with H_2O_2. *Nanomaterials* **2020**, *10*, 114. [CrossRef]

56. Ohkubo, Y.; Aoki, T.; Seino, S.; Mori, O.; Ito, I.; Endo, K.; Yamamura, K. Radiolytic Synthesis of Pt-Particle/ABS Catalysts for H_2O_2 Decomposition in Contact Lens Cleaning. *Nanomaterials* **2017**, *7*, 235. [CrossRef]
57. Ohkubo, Y.; Aoki, T.; Seino, S.; Mori, O.; Ito, I.; Endo, K.; Yamamura, K. Improved Catalytic Durability of Pt-Particle/ABS for H_2O_2 Decomposition in Contact Lens Cleaning. *Nanomaterials* **2019**, *9*, 342. [CrossRef]
58. Singh, K.S.W.; Rouquerol, J.; Bergeret, G.; Gallezot, P.; Vaarkamp, M.; Koningsberger, D.C.; Datye, A.K.; Niemantsverdriet, J.W.; Butz, T.; Engelhardt, G.; et al. *Handbook of Heterogeneous Catalysis*; Wiley: Hoboken, NJ, USA, 1997; pp. 427–582. [CrossRef]
59. Narayanan, R.; El-Sayed, M.A. Shape-Dependent Catalytic Activity of Platinum Nanoparticles in Colloidal Solution. *Nano Lett.* **2004**, *4*, 1343–1348. [CrossRef]
60. Serra-Maia, R.; Winkler, C.; Murayama, M.; Tranhuu, K.; Michel, F.M. Abundance and Speciation of Surface Oxygen on Nanosized Platinum Catalysts and Effect on Catalytic Activity. *ACS Appl. Energy Mater.* **2018**, *1*, 3255–3266. [CrossRef]

Disclaimer/Publisher's Note: The statements, opinions and data contained in all publications are solely those of the individual author(s) and contributor(s) and not of MDPI and/or the editor(s). MDPI and/or the editor(s) disclaim responsibility for any injury to people or property resulting from any ideas, methods, instructions or products referred to in the content.